Title

Dynamic restructuring drives catalytic activity on nanoporous gold—silver alloy catalysts

Journal

Nature Materials, 16(5)

ISSN

1476-1122

Authors

Zugic, Branko

Wang, Lucun

Heine, Christian

et al.

Publication Date

2017-05-01

DOI

10.1038/nmat4824

Peer reviewed

ARTICLES
PUBLISHED ONLINE: 19 DECEMBER 2016 | DOI: 10.1038/NMAT4824
nature materials

Dynamic restructuring drives catalytic activity on nanoporous gold–silver alloy catalysts

Branko Zugic[1], Lucun Wang[1], Christian Heine[2], Dmitri N. Zakharov[3], Barbara A. J. Lechner[2], Eric A. Stach[3], Juergen Biener[4], Miquel Salmeron[2], Robert J. Madix[5] and Cynthia M. Friend[1,5]*

Bimetallic, nanostructured materials hold promise for improving catalyst activity and selectivity, yet little is known about the dynamic compositional and structural changes that these systems undergo during pretreatment that leads to efficient catalyst function. Here we use ozone-activated silver–gold alloys in the form of nanoporous gold as a case study to demonstrate the dynamic behaviour of bimetallic systems during activation to produce a functioning catalyst. We show that it is these dynamic changes that give rise to the observed catalytic activity. Advanced *in situ* electron microscopy and X-ray photoelectron spectroscopy are used to demonstrate that major restructuring and compositional changes occur along the path to catalytic function for selective alcohol oxidation. Transient kinetic measurements correlate the restructuring to three types of oxygen on the surface. The direct influence of changes in surface silver concentration and restructuring at the nanoscale on oxidation activity is demonstrated. Our results demonstrate that characterization of these dynamic changes is necessary to unlock the full potential of bimetallic catalytic materials.

Bimetallic catalysts present unique opportunities for tuning product selectivity and increasing energy efficiency in the chemicals industry. The dynamic response of bimetallic materials to their environment[1–3] strongly indicates that changes in structure and surface composition control catalytic function, demonstrating the need for the investigation of such materials using *in situ* techniques. Gold-based alloys[4–8], in particular, have emerged as promising catalysts for selective alcohol oxidation, esterification, and amidization reactions.

Nanoporous gold (npAu) is a well-defined, bimetallic, single-phase solid solution alloy that is not complicated by lattice mismatch, intermetallic compounds, or metal-support interactions. It is highly active and selective for oxygen-assisted coupling of both alcohols and amines[9,10]. A key step in these O-assisted reactions is the dissociation of O_2 to adsorbed O, which is required for the initiation of reaction. Although the gold-rich surface is needed for high reaction selectivity, pure metallic gold does not activate O_2 with a measurable rate[11,12], whereas this dilute Ag–Au alloy (npAu) does. Activation of the npAu by flowing ozone and subsequently a mixture of methanol and O_2 is required for reproducible and robust catalytic function[9,10,13]. The catalyst activated in this way has unique properties, being inactive for sustained, catalytic CO oxidation[13] (although npAu in other forms is)[14,15] but highly active for selective oxidative alcohol coupling. This difference makes the following results distinct from the recent studies by Fujita *et al.*[16] that probed structural rearrangements of npAu during CO oxidation on as-prepared npAu materials.

A critical question addressed here is how and why the ozone activation process changes the catalyst. We demonstrate that critical structural and compositional changes at the surface of npAu (due to the ozone activation and subsequent reduction by methanol) govern the development of its unique catalytic activity by using *in situ* X-ray and electron microscopy techniques and transient kinetic measurements. All experiments were performed under similar conditions of pressure, gas composition, and temperature so that they could be directly correlated to provide critical details about the catalyst structure and composition. We show that *in situ* ozone pretreatment creates a silver-rich oxide layer on the npAu surface that is highly reactive to both CO and CH_3OH to yield the non-selective oxidation product CO_2. Removal of this reactive oxygen by CO leads to restructuring that generates a gold–silver alloy and a distinct oxygen species stabilized at Ag–Au alloy sites. This species can be removed by CH_3OH to exclusively form selective oxidation products (its removal causes further migration of Ag into the subsurface) and regenerated by exposure of the alloy surface to O_2. The creation of this species is strongly linked to Ag migration facilitated by ozone treatment, which leads to a material that is functionally distinct from npAu that is highly active for CO oxidation. This study clearly demonstrates that the behaviour of alloy catalysts can be tuned using carefully constructed catalyst pretreatment methods. In addition, this work demonstrates how catalyst activation—the transformation of a material into a robust and long-lived catalyst—is critical to the development of efficient catalytic processes.

Results and discussion

Exposure of ozone-treated npAu to a reactant stream of methanol (6.5%) and oxygen (20%) under catalytic oxidation conditions results in the transient production of CO_2 (combustion) before selective coupling to methyl formate commences (Fig. 1). The initial reaction in the flow reactor is the near-complete combustion of methanol to CO_2 as the temperature approaches 150 °C. The onset of CO_2 is sudden and accompanied by a release of heat, causing the temperature to overshoot, thus suggesting an autocatalytic process.

[1]Department of Chemistry and Chemical Biology, Harvard University, Cambridge, Massachusetts 02138, USA. [2]Materials Science Division, Lawrence Berkeley National Laboratory, Berkeley, California 94720, USA. [3]Center for Functional Nanomaterials, Brookhaven National Laboratory, Upton, New York 11973, USA. [4]Nanoscale Synthesis and Characterization Laboratory, Lawrence Livermore National Laboratory, Livermore, California 94550, USA. [5]Paulson School of Engineering and Applied Sciences, Harvard University, Cambridge, Massachusetts 02138, USA. *e-mail: friend@fas.harvard.edu

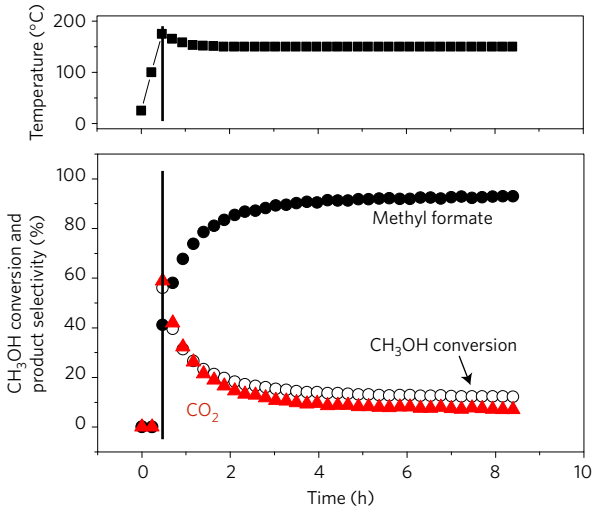

Figure 1 | Activation of npAu for selective methanol oxidation. Final activation of ozone-treated npAu occurs by flowing the methanol/O_2 reaction mixture over the catalyst while the temperature is ramped to the operating temperature of 150 °C. During activation, combustion first predominates followed by a switch to selective formation of methyl formate with nearly 100% selectivity. The solid line indicates the point at which a temperature of 150 °C is reached, and the corresponding onset of reaction. The activity for selective production of methyl formate remains stable for at least several weeks (see ref. 13.).

After this initial combustion phase, methyl formate becomes the dominant product, eventually reaching >95% selectivity. The activity and selectivity are sustained for a long period—up to several weeks[13]. Furthermore, the three different forms of nanoporous Au used—ingots, thin foils, and hollow shells—all exhibit the same activation behaviour and catalytic activity[13]. The correspondence in catalytic behaviour demonstrates that the catalytic behaviour is dictated by the nano- and atomic-scale behaviour of the material and not the larger-scale architecture.

Combustion of methanol is also initially predominant when the ozone-treated npAu catalyst is exposed to very short pulses (<1 ms) of either methanol alone or a methanol–CO mixture (Fig. 2a,c and Supplementary Fig. 1). The rapid transition from CO_2 to selective oxidation indicates that there are two types of oxygen species on the surface—one responsible for combustion and the other for partial oxidation. Due to extremely short contact times in the pulse reactor, the dominant selective oxidation product is formaldehyde, rather than methyl formate. In the flow reactor, the same catalyst yielded methyl formate with high selectivity, as previously reported. It is well known that the first step in the catalytic cycle for methanol self-coupling is activation of methanol to formaldehyde[17,18]; the transient experiments probe the initial step in the reaction pathway that governs the steady-state reaction. The difference in product selectivity in the titration with methanol pulses and in steady flow is related to the large difference in contact times (10^{-4} s versus 10^{-1} s, respectively) with the catalyst and will be addressed in a separate paper[19].

In a separate experiment, the surface oxygen resulting from O_3-treatment of the npAu surface was first titrated with 100 pulses of CO to remove the surface O responsible for combustion. Exposure to methanol pulses then directly yields partial oxidation products and not the initial methanol combustion (indicated by the dashed line in Fig. 2b). This result indicates that the chemical behaviour of the adsorbed O is not sensitive to the method of reduction of the more reactive oxygen that promotes combustion. In addition, a pause during the continuous pulsing of either CO or CH_3OH has minimal effect on the evolution of the different products as the pulses are resumed, indicating that the different states of surface oxygen from O_3 treatment are not inter-convertible.

When the O_3-treated npAu catalyst is first exposed to pulses of a mixture of CO and CH_3OH simultaneously, both reactants are completely consumed and CO_2 is the only product observed (Fig. 2c,d). After most of the surface oxygen (95%) is reacted away through CO_2 production, the CO conversion rapidly drops to zero. Concomitantly, selective reaction of methanol to formaldehyde and methyl formate commences without CO_2 formation. The pattern of methanol reactivity is essentially the same whether it is pulsed alone or in the presence of CO (Fig. 2).

These results clearly demonstrate that there are two chemically distinct types of oxygen species formed during the O_3 treatment of the catalyst and that only the minority oxygen species, present on the surface at low concentrations, is responsible for the selective oxidation of methanol. Furthermore, the catalyst facilitates the dissociation of O_2 after complete reaction of the 'selective' oxygen via reaction with methanol. Exposure of this material to dioxygen produces adsorbed O, but only from reaction with the minority sites[19]; this adsorbed oxygen is unreactive with CO but reacts readily with methanol to give selective oxidation products. This is in agreement with previous studies of ozone-activated npAu[13].

The primary morphological change observed by *in situ* aberration-corrected transmission electron microscopy (TEM) after ozone treatment is the formation of an amorphous thin film oxide on the surface of the npAu (Fig. 3 and Supplementary Fig. 2). The oxide covers >80% of the npAu surface (Fig. 3b,c) with a thickness of 1.1 ± 0.1 nm. This oxide is not present in as-prepared npAu (that is, not treated with ozone). Additionally, islands (Fig. 3c) and embedded oxides (Fig. 3d) are observed on and within the npAu ligaments, respectively. The islands are two atomic layers in height and 2–6 nm in diameter. The observable inter-planar spacing within these structures is ~0.31 nm (compared with 0.24 nm for the (111) spacing of metallic Au and Ag), which suggests formation of metal oxides (Supplementary Table 1)[20,21]. These findings are in line with previous studies of textured Au(111) surfaces that indicate that treatment with ozone results in the formation of chemisorbed oxygen species and three-dimensional gold oxides of ~1.5 nm in thickness[22]. The disordered, embedded oxides also observed by TEM (Fig. 3d) are ~1–2 nm deep and ~6–8 nm in diameter.

In addition to these structural changes, high-angle annular dark-field scanning transmission electron microscopy/electron energy-loss spectroscopy (HAADF-STEM/EELS) analysis clearly shows that the ozone treatment causes the aggregation of Ag oxides at the npAu surface. This is seen in the HAADF-STEM image (Fig. 3d) as regions of lower density (that is, lower *Z* contrast). Further analysis by EELS (Fig. 3e and Supplementary Fig. 3) shows that these regions are high in Ag and O concentration. By contrast, little to no Ag is detected in the npAu away from these regions.

All of the amorphous oxide layer is removed by *in situ* reduction of the O_3-treated npAu with CO (0.1 torr CO at 150 °C for 30 min) in the environmental TEM (E-TEM Fig. 4a–c). Since catalytic CO oxidation is not sustained, we infer that the oxide is not reformed under operating catalytic conditions. The removal of the oxide layer is accompanied by formation of small, irregular nanoparticles on highly stepped regions of npAu (Fig. 4b,c). The newly formed particles are irregularly shaped with large variations in the atomic spacing (Fig. 4b). The larger lattice spacing (~0.32 nm), determined by Fourier transform analysis, corresponds to that of gold and silver oxides (Supplementary Table 1).

Further reduction of the npAu surface by methanol results in the growth of crystalline nanoparticles at the surface to 2–2.5 nm in diameter (Fig. 4d–f). In addition to the increase in diameter, these structures appear more ordered and show more distinct facets, as shown in Fig. 4f. The particle aspect ratio (height to width ratio at the base of the particle) also changes from 0.7 after

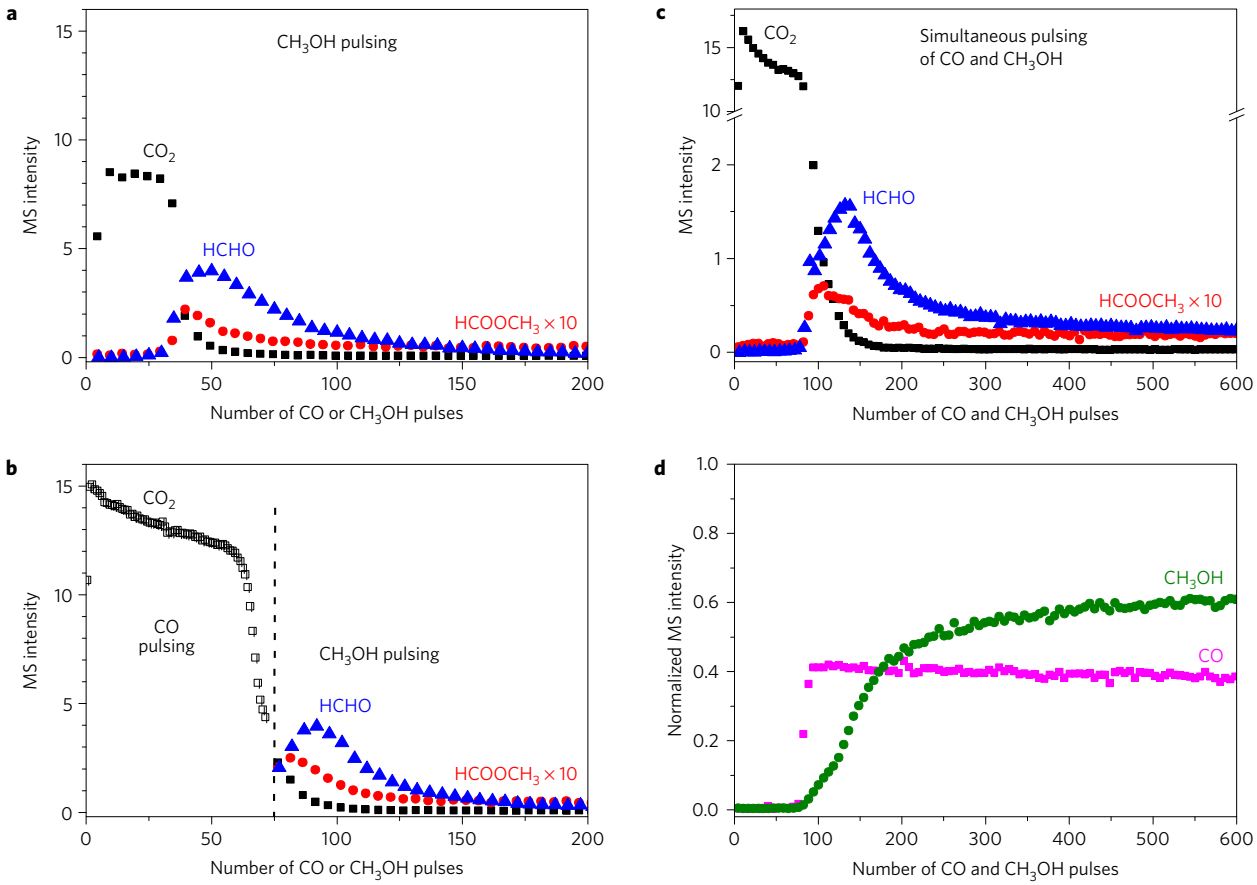

Figure 2 | Pulsed experiments over ozone-treated npAu. Transient (pulsed) experiments over O_3-treated npAu at 150 °C demonstrate that there are two chemically distinct oxygen species present on the surface: one responsible for combustion to CO_2 and the other for selective CH_3OH oxidation to HCHO and $HCOOCH_3$. **a**, During CH_3OH pulsing over O_3-treated npAu, complete combustion to CO_2 is observed initially; after ~25 pulses, combustion rapidly diminishes and selective CH_3OH oxidation to formaldehyde is observed; the reaction ceases after ~200 pulses. **b**, Non-selective oxygen species can be removed by titration of highly reactive oxygen on O_3-treated npAu by exposure to 75 pulses of CO; CH_3OH pulsing thereafter yields only selective oxidation products. **c**,**d**, Titration of surface oxygen on O_3-treated npAu by simultaneously pulsing methanol and CO onto O_3-treated npAu yields an identical pattern of reactivity—initial reaction of both CO and CH_3OH to CO_2, followed by reaction of only CH_3OH to selective oxidation products (the pulse sizes of CO and CH_3OH are reduced by 50% relative to **a** and **b** to keep total reactant per pulse constant).

CO treatment to 0.3 after CH_3OH exposure. These changes may indicate a higher propensity for the particles to realloy into the bulk at low oxygen concentrations at the surface. Furthermore, there is a clear alignment of the crystal planes in the particle and ligament, suggesting that the particles are more metallic in nature.

The oxidation and enrichment of Ag at the npAu surface after ozone treatment is demonstrated using ambient-pressure X-ray photoelectron spectroscopy (AP-XPS; Fig. 5 and Supplementary Tables 2–4). Essentially all Ag and 80% of Au within the 0.5 nm sampling depth (that is, inelastic mean free path through Au)[23] are initially oxidized by ozone at 150 °C (Fig. 5a and Supplementary Table 3). Immediately following the ozone treatment, the Ag/Au atomic ratio is 0.46 (a 30% increase relative to fresh npAu), even though the bulk npAu Ag concentration is only ~3 at% based on energy dispersive X-ray spectroscopy[13]. Furthermore, all of the detectable silver on the surface is fully oxidized to AgO (ref. 24).

The presence of chemically distinct oxygen species after ozone treatment is also detected using the AP-XPS. The O1*s* binding energy is in agreement with previously reported oxygen states for bulk Au and Ag oxides (Fig. 5a and Supplementary Table 4, O_x species)[22,25–27]. Following reduction by CO (0.1 torr, 150 °C), ~90% of this oxidic oxygen is removed (Fig. 5b), which correlates with the CO pulse titration results described above and with the restructuring of the materials in E-TEM. These results further confirm that CO readily reacts with the oxidic oxygen. A new oxygen species (O_{sel}) with a binding energy of 531.5 eV appears in conjunction with the reduction (Fig. 5b and Supplementary Fig. 4). This oxygen species persists until exposure to CH_3OH (Fig. 5c) and it is attributed to the second state of O that leads to selective oxidation of methanol. There is also a residual state of oxygen (O_{res}) with a binding energy of 532 eV that remains in the surface region even after the 30 min exposure to methanol at 150 °C; this species is attributed to oxygen in the subsurface[28]. Depth profiling of the npAu over the course of these experiments indicates that the oxidized Ag and Au species are present only at the outer surface region and that realloying of Ag into the bulk takes place during the sequential reduction by CO and CH_3OH (Supplementary Fig. 5).

Reduction of the O_3-treated npAu also leads to a significant rearrangement of gold and silver within the surface region such that the Ag/Au ratio decreases significantly from 0.46 to 0.26 after reduction of the material by CO (Figs 5b and 6). A corresponding increase in the abundance of undercoordinated Au ($Au_{u/c}$), metallic Au (Au^0), and Ag-alloyed Au (Au_{alloy}) is also observed (Fig. 6 and Supplementary Information)[29]. Nevertheless, some Ag_2O remains and the ratio of the Au_{alloy} to Ag_{alloy} is found to be ~1. Subsequent reduction by CH_3OH (Fig. 5c) results in a further reduction of silver content in the surface (to an Ag/Au ratio of 0.11), a further increase in the undercoordinated gold sites, and the complete removal of the

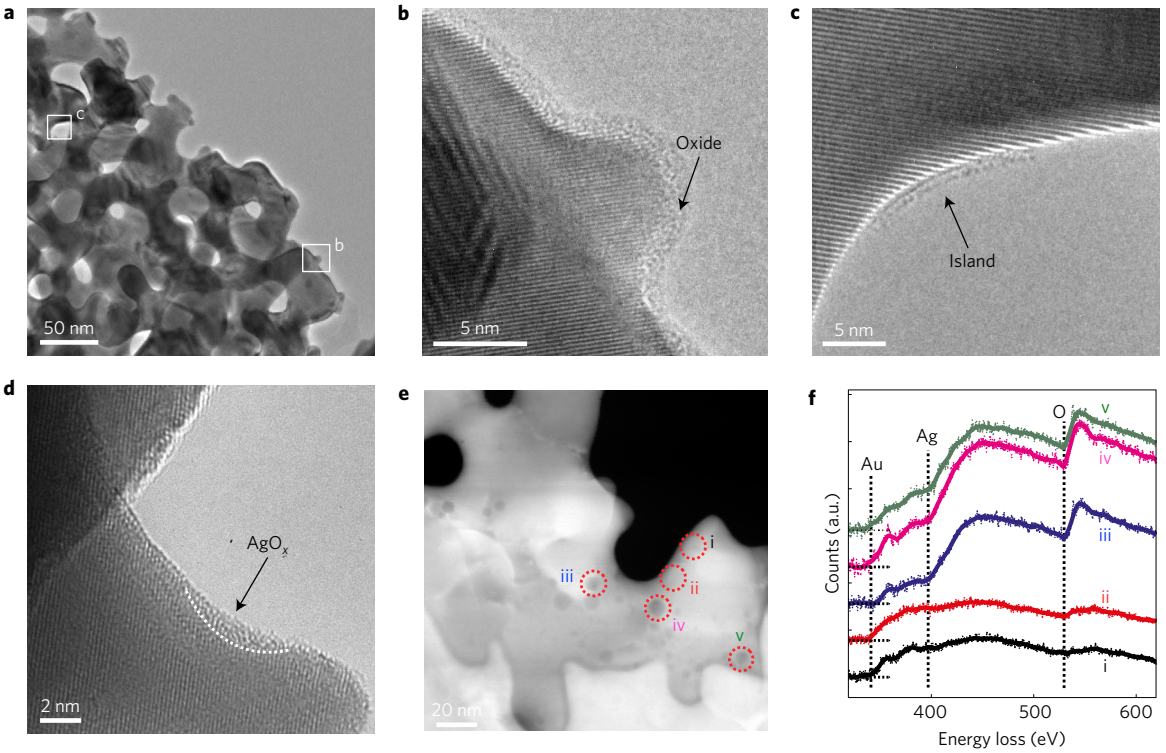

Figure 3 | E-TEM analysis of npAu after ozone treatment. *In situ* aberration-corrected TEM images demonstrate that npAu is oxidized by O_3 treatment in a flow reactor at 150 °C for 1 h. **a**, Low-magnification image of the material showing the pore and ligament structure. **b**, High-resolution image of a representative spot on the material showing the resolved lattice of the ligaments and a layer of amorphous oxide after O_3 treatment. **c**, In some areas, crystalline islands are visible on the npAu surface in the high-magnification images. **d**, *Ex situ* aberration-corrected TEM image showing the presence of amorphous oxides embedded into the npAu ligament. **e**, HAADF-STEM image showing areas of varying contrast on the npAu surface, corresponding to features seen by TEM in **d**. **f**, EELS analysis of various spots from **e**, showing that the darker areas are regions of high Ag and O concentration relative to the rest of the npAu surface.

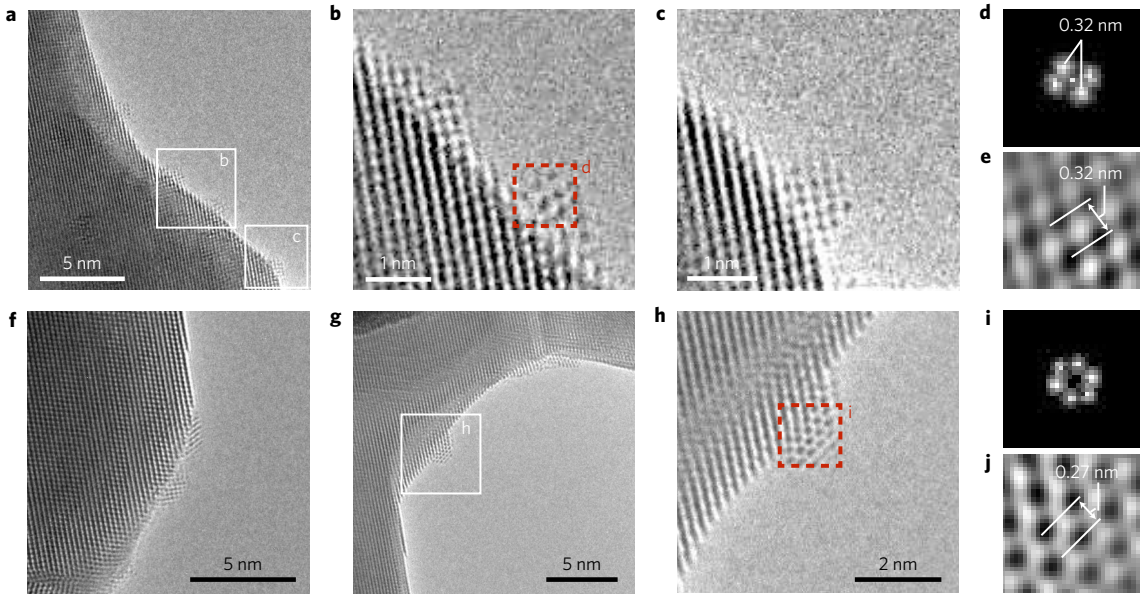

Figure 4 | E-TEM analysis of npAu during CO and CH_3OH exposure. *In situ* removal of the oxide layer and formation of nanoparticles due to reduction of ozone-treated npAu by CO and CH_3OH is observed in aberration-corrected E-TEM images. **a**–**c**, Exposure of O_3-treated npAu to 0.1 torr CO at 150 °C for 30 min leads to removal of the oxide film and precipitation of defective nanoparticles (1–1.6 nm in diameter) with an expanded lattice. **d**, Masked fast Fourier transform of the region marked in **b**, showing the two types of lattice spacing observed. **e**, Inverse fast Fourier transform of **d**, showing the oxidic 0.32 nm spacing corresponding to the particle in **b**. **f**–**h**, Highly crystalline metallic nanoparticles form following further reduction by 0.1 torr CH_3OH at 150 °C for 30 min. **i**, Masked fast Fourier transform of the region marked in **h**. **j**, Inverse fast Fourier transform of **i**, showing a typical Au(111)-type arrangement. All images were obtained at 25 °C and under vacuum conditions after reduction treatments; no beam effects were observed during imaging. Note: the observed particle density and shape on the npAu surface accounts for ~11% of the npAu surface area after CO reduction and ~27% after CH_3OH reduction.

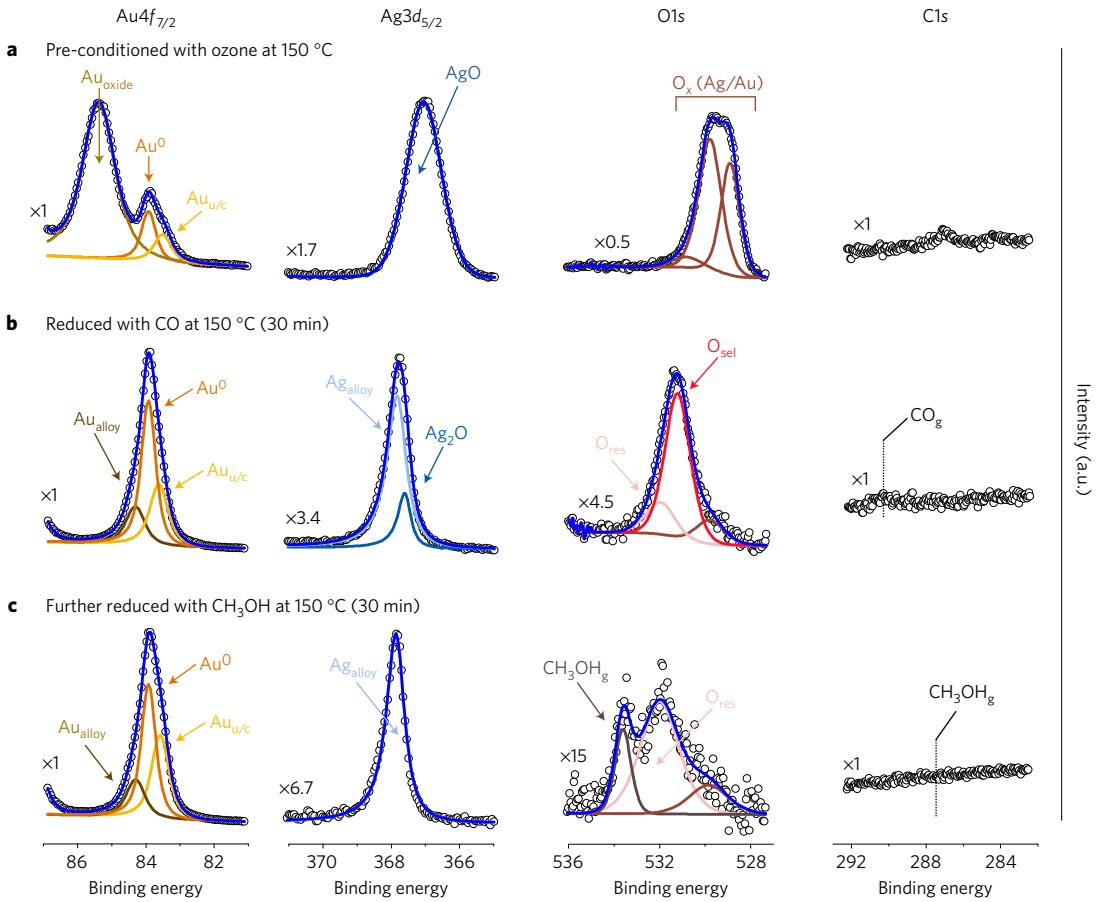

Figure 5 | AP-XPS analysis of npAu. AP-XPS data demonstrate that two distinct O species are present on O_3-treated npAu and that the surface Ag concentration decreases as a result of reduction by CO and CH_3OH. **a**, After the ozone treatment in 0.3 torr 2% O_3/O_2 at 150 °C for 30 min, both Au and Ag are oxidized (labelled Au_{oxide} and AgO) and the O1s contributions are typical of bulk Au and Ag oxides (labelled O_x). **b**, After reduction by 0.1 torr CO at 150 °C for 30 min, Au is completely reduced to Au^0 and there is an increase in undercoordinated Au sites ($Au_{u/c}$); some AgO is reduced to Ag_2O while the majority is realloyed with Au (Ag_{alloy}); a new O1s contribution is observed, thought to be responsible for selective CH_3OH oxidation (O_{sel}). **c**, Further reduction by 0.1 torr CH_3OH at 150 °C for 30 min shows that the remaining Ag_2O is reduced, there is a further increase in undercoordinated Au sites ($Au_{u/c}$), and only a small amount of residual, subsurface oxygen remains (O_{res}). The kinetic energy for all spectra was kept at 200 eV, corresponding to an inelastic mean free path of 0.5 nm in Au.

Ag_2O phase (Fig. 6). In light of the E-TEM results, we attribute the increase in undercoordinated Au sites to the formation and growth of small crystalline particles on the npAu surface (Fig. 4).

This comprehensive investigation of the activation of npAu using ozone treatment followed by exposure to reductants elucidates the key role that catalyst preparation and pretreatment has on the resulting activity. The initial treatment with ozone substantially enriches the surface in Ag by more than a factor of 10 compared with the bulk average and it removes adventitious carbon from the npAu, as demonstrated previously[9]. The treatment with ozone also leads to an excess of oxygen at the surface: this yields an oxidic material that promotes combustion of methanol and other alcohols[10,13]. This oxidic state can also be reduced by reaction with CO.

The first state of reduction by CO leads to removal of the oxidic oxygen and redistribution of both Ag and Au. The surface remains enriched in Ag with disordered particles that are on the order of a few nanometres in diameter. The second state of oxygen that persists does not react with CO; rather, it induces selective oxidation of methanol and most likely other alcohols. The reason that this oxygen does not react with CO, but does react with methanol is not known and is a topic for further study. A possible explanation is that the disordered nature of the Ag-containing nanoparticles (Fig. 4a–e) results in strong electron depletion at the surface, leading to the formation of associative oxygen species (supported by the high AP-XPS binding energies)[30]. Further reduction of the second state of oxygen by methanol leads to additional rearrangement of the surface so that metallic nanoparticles are formed and the Ag/Au ratio is lowered. The pattern of compositional changes indicates that Ag segregation is favoured under highly oxidizing conditions but that it recedes from the surface under reducing conditions. Importantly, the Ag distribution does not revert to the bulk distribution of the as-prepared material. The near-surface region of the active material is still enriched in Ag but not to an extent that oxides form that would lead to over-oxidation (that is, combustion) of the methanol.

These results provide insight into how ozone pretreatment leads to the catalytic function of the activated npAu material under steady-state conditions, when both O_2 and methanol are present. Highly selective formation of methyl formate from methanol occurs under steady-state flow conditions that do not lead to the accumulation of excess oxygen. The surface is enriched in Ag even after reduction with CO, which leaves oxygen that selectively reacts with methanol, suggesting that under steady-state conditions a Ag–Au alloy is present. Indeed, additional AP-XPS data (Supplementary Fig. 6) confirm that the selective oxygen species (O_{sel}), which is the active species for methanol activation, is also present on the sample surface after prolonged exposure to steady-state reaction conditions.

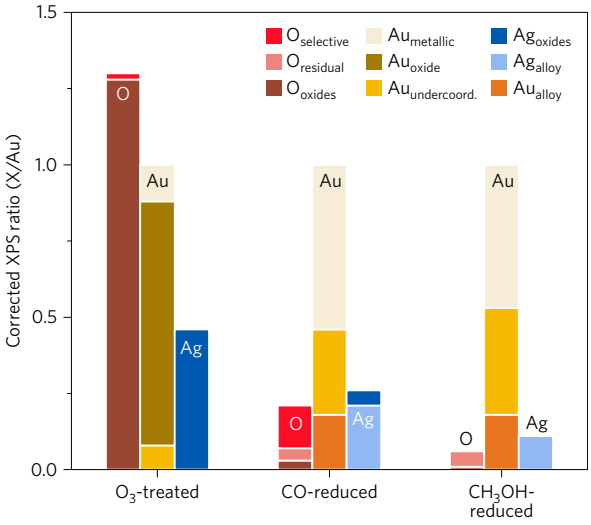

Figure 6 | Changes in the relative surface concentrations of Ag, O and Au. Quantification of Au, Ag and O contributions from Fig. 5 expressed as a ratio relative to the total Au XPS signal intensity (I_x/I_{Au}). After the O_3 treatment, Ag and Au are heavily oxidized. After reduction by CO, the contributions to the AgAu alloy (A_{galloy}), undercoordinated Au, and selective oxygen (O_{sel}) increase. Further reduction by CH_3OH reduces the remaining silver oxides, maintains the A_{galloy} character of Ag and further increases the contribution to undercoordinated Au. Only residual oxygen (O_{res}) remains after CH_3OH reduction.

Conclusions

The enrichment of the surface in Ag indicates that Ag plays a key role in the catalytic function by facilitating O_2 dissociation on the npAu. This assertion is in general agreement with previous studies of npAu[31]; however, the precise atomic arrangement required for O_2 dissociation is yet to be determined. In the absence of other changes such as the step edge/kink site density, the STEM-EELS analysis provides compelling evidence that enrichment in Ag of the nanoparticles formed during the activation process is key to O_2 dissociation. The larger mesoscale structure of the npAu may also be important in forming the active material—for example, the ligament structure is known to create lattice strain and also produces many undercoordinated metal atoms[16,32]. Our results indicate that a combination of structural and compositional factors is important under catalytic conditions. Furthermore, a comparison of these results to those of Fujita *et al.*[16] suggests that different surface configurations of the same parent material (npAu) can yield distinct oxygen species under varying reaction conditions (CO oxidation versus oxidative alcohol esterification).

We expect that the dynamic behaviour reported here is not unique to npAu, but has general implications for other alloy-based catalyst systems. Our results demonstrate that bimetallic nanoporous catalysts can exhibit highly dynamic geometrical and compositional changes during both activation and under reaction conditions that are far more complex than one would anticipate on the basis of planar model systems or small particles. These dynamic changes are responsible for the generation of active regions that control catalyst reactivity, selectivity and long-term stability. Generalization of this concept will require comprehensive studies of structure, composition, and reactivity on other bimetallic catalyst materials. However, we expect that integrating dynamic compositional and morphological changes into catalyst design will open the door to a new area of catalyst development. In the future, theoretical simulations will guide catalyst design by predicting surface-chemistry-induced surface compositional changes. Interesting questions to be answered in this context are: What is the thickness of the surface layer that is affected by surface-chemistry-induced surface diffusion, and what is the role of confinement in stabilizing the ideal surface composition under reaction conditions? Answering these questions will enable a predictive design approach towards next-generation dilute alloy catalysts with tailored surface compositions.

Methods

Methods, including statements of data availability and any associated accession codes and references, are available in the online version of this paper.

Received 2 January 2016; accepted 15 November 2016; published online 19 December 2016

References

1. Behrens, M. *et al*. The active site of methanol synthesis over $Cu/ZnO/Al_2O_3$ industrial catalysts. *Science* **336,** 893–897 (2012).
2. Xin, H. L. *et al*. Revealing the atomic restructuring of Pt–Co nanoparticles. *Nano Lett.* **14,** 3203–3207 (2014).
3. Tao, F. *et al*. Reaction-driven restructuring of Rh–Pd and Pt–Pd core–shell nanoparticles. *Science* **322,** 932–934 (2008).
4. Brett, G. L. *et al*. Selective oxidation of glycerol by highly active bimetallic catalysts at ambient temperature under base-free conditions. *Angew. Chem.* **123,** 10318–10321 (2011).
5. Della Pina, C., Falletta, E. & Rossi, M. Highly selective oxidation of benzyl alcohol to benzaldehyde catalyzed by bimetallic gold–copper catalyst. *J. Catalys.* **260,** 384–386 (2008).
6. Whiting, G. T. *et al*. Methyl formate formation from methanol oxidation using supported gold–palladium nanoparticles. *ACS Catalys.* **5,** 637–644 (2015).
7. Kotionova, T. *et al*. Oxidative esterification of homologous 1,3-propanediols. *Catalys. Lett.* **142,** 1114–1120 (2012).
8. Suzuki, K. *et al*. Aerobic oxidative esterification of aldehydes with alcohols by gold–nickel oxide nanoparticle catalysts with a core–shell structure. *ACS Catalys.* **3,** 1845–1849 (2013).
9. Stowers, K. J., Madix, R. J. & Friend, C. M. From model studies on Au(111) to working conditions with unsupported nanoporous gold catalysts: oxygen-assisted coupling reactions. *J. Catalys.* **308,** 131–141 (2013).
10. Wang, L.-C. *et al*. Exploiting basic principles to control the selectivity of the vapor phase catalytic oxidative cross-coupling of primary alcohols over nanoporous gold catalysts. *J. Catalys.* **329,** 78–86 (2015).
11. Sault, A. G., Madix, R. J. & Campbell, C. T. Adsorption of oxygen and hydrogen on Au(110)-(1 × 2). *Surf. Sci.* **169,** 347–356 (1986).
12. Meyer, R., Lemire, C., Shaikhutdinov, S. K. & Freund, H. J. Surface chemistry of catalysis by gold. *Gold Bull.* **37,** 72–124 (2011).
13. Personick, M. L. *et al*. Ozone-activated nanoporous gold: a stable and storable material for catalytic oxidation. *ACS Catalys.* **5,** 4237–4241 (2015).
14. Xu, C. *et al*. Low temperature CO oxidation over unsupported nanoporous gold. *J. Am. Chem. Soc.* **129,** 42–43 (2007).
15. Biener, M. M. *et al*. ALD functionalized nanoporous gold: thermal stability, mechanical properties, and catalytic activity. *Nano Lett.* **11,** 3085–3090 (2011).
16. Fujita, T. *et al*. Atomic origins of the high catalytic activity of nanoporous gold. *Nat. Mater.* **11,** 775–780 (2012).
17. Xu, B., Liu, X., Haubrich, J., Madix, R. J. & Friend, C. M. Selectivity control in gold-mediated esterification of methanol. *Angew. Chem. Int. Ed.* **48,** 4206–4209 (2009).
18. Xu, B., Haubrich, J., Freyschlag, C. G., Madix, R. J. & Friend, C. M. Oxygen-assisted cross-coupling of methanol with alkyl alcohols on metallic gold. *Chem. Sci.* **1,** 310–316 (2010).
19. Wang, L. C. *et al*. Active sites for methanol partial oxidation on nanoporous gold catalysts. *J. Catalys.* **344,** 778–783 (2016).
20. in *Non-tetrahedrally Bonded Elements and Binary Compounds I* Vol. 41C (eds Madelung, O., Rössler, U. & Schulz, M.) 1–3 (Springer, 1998).
21. Jones, P. G. *et al*. Gold(III) oxide. *Acta Crystallogr. B* **35,** 1435–1437 (1979).
22. Krozer, A. & Rodahl, M. X-ray photoemission spectroscopy study of UV/ozone oxidation of Au under ultrahigh vacuum conditions. *J. Vac. Sci. Technol. A* **15,** 1704–1707 (1997).
23. Tanuma, S., Powell, C. J. & Penn, D. R. Calculations of electron inelastic mean free paths. *Surf. Interface Anal.* **21,** 165–176 (1994).
24. Kaspar, T. C., Droubay, T., Chambers, S. A. & Bagus, P. S. Spectroscopic evidence for Ag(III) in highly oxidized silver films by X-ray photoelectron spectroscopy. *J. Phys. Chem. C* **114,** 21562–21571 (2010).

25. Hammond, J. S. & Gaarenstroom, S. W. X-ray photoelectron spectroscopic studies of cadmium– and silver–oxygen surfaces. *Anal. Chem.* **47,** 2193–2199 (1975).
26. Hoflund, G. B., Hazos, Z. F. & Salaita, G. N. Surface characterization study of Ag, AgO, and Ag_2O using x-ray photoelectron spectroscopy and electron energy-loss spectroscopy. *Phys. Rev. B* **62,** 11126–11133 (2000).
27. Xu, B., Siler, C. G. F., Madix, R. J. & Friend, C. M. Ag/Au mixed sites promote oxidative coupling of methanol on the alloy surface. *Chem. Eur. J.* **20,** 4646–4652 (2014).
28. Boronin, A. I., Koscheev, S. V. & Zhidomirov, G. M. XPS and UPS study of oxygen states on silver. *J. Electron Spectrosc. Relat. Phenom.* **96,** 43–51 (1998).
29. Tyson, C. C. *et al*. Charge redistribution in Au–Ag alloys from a local perspective. *Phys. Rev. B* **45,** 8924–8928 (1992).
30. Kibis, L. S. *et al*. The investigation of oxidized silver nanoparticles prepared by thermal evaporation and radio-frequency sputtering of metallic silver under oxygen. *Appl. Surf. Sci.* **257,** 404–413 (2010).
31. Moskaleva, L. V., Weiss, T., Klüner, T. & Bäumer, M. Chemisorbed oxygen on the Au(321) surface alloyed with silver: a first-principles investigation. *J. Phys. Chem. C* **119,** 9215–9226 (2015).
32. Fujita, T. *et al*. Atomic observation of catalysis-induced nanopore coarsening of nanoporous gold. *Nano Lett.* **14,** 1172–1177 (2014).

Acknowledgements

This work was supported as part of the Integrated Mesoscale Architectures for Sustainable Catalysis, an Energy Frontier Research Center funded by the US Department of Energy, Office of Science, Basic Energy Sciences under award no. DE-SC0012573. Work at LLNL was performed under the auspices of the US Department of Energy by LLNL under Contract DE-AC52-07NA27344. This research used resources of the Center for Functional Nanomaterials, which is a US DOE Office of Science Facility, at Brookhaven National Laboratory under Contract No. DE-SC0012704. It also used resources of the Advance Light Source, which is supported by the Office of Science of the US DOE under Contract No. DE-AC02-05CH11231. We thank H. Bluhm for advice on the preparation of the AP-XPS experiments and H. Xin for valuable discussion regarding the EELS data.

Author contributions

C.M.F., R.J.M., J.B. and B.Z. conceived and designed the experimental plan. B.Z. conducted the flow reactor experiments. B.Z. and J.B. prepared the npAu samples. L.W. conceived and conducted the TAP reactor experiments. C.H., M.S., B.A.J.L. and B.Z. conceived and conducted the AP-XPS experiments and analysed the XPS data. E.A.S., D.N.Z. and B.Z. planned and conducted E-TEM experiments. B.Z. wrote the initial draft of the manuscript. All authors discussed the results and contributed to the final preparation of the manuscript.

Additional information

Supplementary information is available in the online version of the paper. Reprints and permissions information is available online at www.nature.com/reprints. Correspondence and requests for materials should be addressed to C.M.F.

Competing financial interests

The authors declare no competing financial interests.

Methods

Sample preparation. Nanoporous gold (npAu) ingots were prepared by free corrosion of $Ag_{70}Au_{30}$ gold ingots in 70% nitric acid (Sigma Aldrich) for 48 h. The initially prepared Ag–Au ingots were homogenized by annealing in argon for 140 h at 875 °C. After cutting, rolling and stamping, the samples were annealed for a second time of 4 h at 800 °C. After dealloying, the samples were washed thoroughly with deionized water, and dried in air. Nanoporous gold hollow microspheres were prepared by a polystyrene sphere templating method previously reported by our group (see Supplementary Information). Nanoporous gold foils for TEM analysis were prepared by dealloying $Ag_{85}Au_{15}$ leaves in nitric acid. All samples had a residual Ag concentration of ∼3 at% after nitric acid leaching, as determined by energy-dispersive spectroscopy analysis.

Reactor activation and testing. All npAu catalysts were activated and tested in a quartz tube reactor housed within a temperature-controlled tubular furnace operated at atmospheric pressure. Ultrahigh-purity gases (He, O_2) were supplied to the reactor by mass flow controllers (MKS). Ozone treatment was performed by flowing ozone (2–3%) in an O_2 gas at 70 ml min^{-1} over the catalyst at room temperature for ∼30 min, followed by ramping the temperature to 150 °C at 10 °C min^{-1} and holding for 1 h. The sample was cooled in the ozone mixture and purged with He at room temperature for at least 1 h. Activation and testing of the sample in reaction gas was then immediately performed in 6.5% CH_3OH–20% O_2 (balance He) at 50 ml min^{-1} using a temperature ramp from 298 K (25 °C) to 425 K (150 °C) at 10 °C min^{-1}. Methanol was supplied by a saturated He stream directed through a bubbler, followed by a temperature-controlled condenser. The effluent gas was continuously monitored by an online GC–MS (Agilent 5975C and Agilent 7890A) equipped with HP-PLOT Q and CARBONPLOT columns.

TAP reactor testing. The pulse experiments were carried out in a commercial temporal analysis of products (TAP)-2 reactor (see Supplementary Information for details). In a typical pulse response experiment a narrow pulse of reactant gas (about 10^{-8} mol per pulse, pulse width 0.135 ms) was injected into a packed-bed microreactor using a high-speed, magnetically controlled pulse valve. The microreactor was a quartz tubular reactor with a length of 38 mm and a diameter of 6.35 mm, housing an internal thermocouple. The microreactor sat on top of a high-throughput vacuum chamber (10^{-8}–10^{-9} torr) containing a RGA200 mass spectrometer, which was used to detect the effluent from the reactor. The npAu catalyst was sandwiched in a thin-zone configuration in the middle of the microreactor packed among inert quartz particles with diameters between 250 and 300 μm. Pulse sizes were chosen to ensure Knudsen flow throughout the reactor.

Ambient-pressure XPS. Ambient-pressure X-ray photoelectron spectroscopy (AP-XPS) experiments were conducted at Beamline 11.0.2 at the Advanced Light Source at Lawrence Berkeley National Laboratory. A nanoporous gold ingot was previously treated in a flow reactor in 2% O_3 (in O_2) at 150 °C for 1 h. The treated ingot was loaded onto a ceramic button heater, mounted within the AP-XPS chamber at Beamline 11.0.2. See Supplementary Information for experimental and analysis details.

Environmental TEM. Environmental-TEM (E-TEM) studies were performed at the Center for Functional Nanomaterials at Brookhaven National Laboratory using an FEI Titan aberration-corrected TEM operating at 300 kV. The instrument has a base pressure of 3–4 × 10^{-7} torr. The spatial resolution is <180 pm under E-TEM conditions. Ozone-treated npAu foils were placed on a DENS Solutions heated sample holder by dispersion in deionized water. After drying overnight at room temperature, the holder was inserted into the microscope. Gases and vapours were introduced into the microscope using a gas-handling manifold equipped with dosing valves. See Supplementary Information for experimental details.

Data availability. The authors declare that all of the data supporting the findings of this study are available within the paper and its Supplementary Information files.